Utilizing Magnetic Chitosan Hydrogel Nanocomposite for the Processing, and Treatment of Aquaculture Effluent

Mahmoud S. Kelany[1], Hanan A.E.-A Attia[2], Zaki Z. Sharawy[1]* Eman M. Abbas[1], Hosam Easa Elsaied[1], Fatma H. A. Mustafa[1]

[1]National Institute of Oceanography and Fisheries (NIOF), Cairo, Egypt
[2]Quality Control Department, Oriental Petrochemicals Company, Ninth Industrial Zone
Nowrthwest Gulf of Suez, Ain Sokhna, Suez Egypt
*Corresponding Author: zaki_sharawy@yahoo.com

ARTICLE INFO

ABSTRACT

Water pollution harms the human and marine environment. An optimal water quality is a global target for the well-being of all living organisms including human. Based on this concept, this study focused on the synthesis of magnetite nanoparticles using the wet chemical reduction technique and their incorporation with the preparation of magnetic chitosan hydrogel (CS-HG) nanocomposite. Fourier transform infrared spectroscopy (FT-IR), zeta potential, x-ray diffraction (XRD), x-ray fluorescence (XRF), scanning electron microscopy (SEM) and energy dispersive X-ray (EDX) were used as the main characterization tools. The magnetic CS-HG was applied to different types of multi-pollutant water to test its efficiency in removing different pollutants. Magnetic hydrogel showed high efficiencies (99.17, 98.27, 95.17, 93.9 and 49.59%) toward removing iron, phosphates, nitrite, nitrate and ammonia/ammonium, respectively. This study also investigated the effectiveness of a chemical treatment process by magnetic CS-HG in reducing bacterial populations in a water sample. The initial bacterial count of total coliforms (TC) ranged from 600,000 to 5,500,000CFU/ mL, significantly decreasing to 4,000 to 60,000CFU/ mL after treatment. Similarly, *Pseudomonas* counts were reduced from 25,000 to 50 to 75CFU/ mL. Notably, *Aeromonas* sp. and *Vibrio* sp. were not detected in the samples before or after treatment. Further analysis revealed that some previously identified *Pseudomonas* isolates belong to different bacterial genera, including *Neobacillus novalis*, *Psychrobacillus lasiicapitis*, *Acinetobacter schindleri*, and *Bacillus paramycoides*. Thus, magnetic CS-HG could be applied to clean up different kinds of water.

INTRODUCTION

Maintaining optimal water quality in aquaculture is crucial for the well-being of aquatic organisms like fish and shellfish. Chemical compounds play a pivotal role in enhancing water quality and ensuring the success of aquaculture operations (**Ahmad *et al.,* 2021; Hassan *et al*., 2022a**). While aquaculture is vital for global seafood production, intensive practices can lead to challenges such as nutrient accumulation and disease spread, emphasizing the need for effective water treatment strategies to promote sustainability (**Sharawy *et al*., 2017; Sharawy *et al*., 2022; Abbas *et al*., 2023**).

Synthesized chemical compounds offer valuable tools for addressing these challenges and supporting the conservation of wild fish populations **(Hamilton *et al.,* 2016)**.

Moreover, the synthesized chemical compounds play a crucial role in aquaculture water processing, employing techniques like pH stabilizers to maintain optimal conditions for aquatic species. Specialized compounds also assist in removing harmful toxins, such as ammonia and nitrites, preventing stress and potential mortality among aquatic inhabitants **(Jose Priya & Kappalli, 2023)**. Additionally, synthesized compounds contribute to disease management by targeting specific pathogens, reducing the risk of outbreaks and minimizing the need for reactive interventions. This proactive approach safeguards the health of cultured organisms and minimizes the use of larger quantities of chemicals in aquaculture **(Sundin *et al.,* 2016)**. Similarly, compounds that bind with and neutralize excess nutrients like ammonia and nitrites can limit the availability of resources that bacteria require for growth **(Mansour *et al*., 2022a, b)**. The role of chemical compounds in reducing bacterial numbers in aquaculture wastewater is a critical facet of modern aquaculture management **(Gichana *et al.,* 2018)**. These compounds contribute to maintaining water quality, protecting the health of aquatic organisms, and mitigating the potential environmental impact of intensive aquaculture practices **(El-Sawy *et al*., 2022; Hassan *et al*., 2022b)**. As the aquaculture industry continues to evolve, the responsible utilization of chemical compounds offers a pathway to sustainable and efficient wastewater management, ensuring the coexistence of aquaculture operations with surrounding ecosystems **(Ahmad *et al.,* 2022)**.

Chitosan (CS) is a natural biopolymer that is mostly derived from the deacetylation of chitin. Chitin is the second most abundant biopolymer and is obtained as a waste product from the food industry. CS exhibits biocompatibility, biodegradability, and non-toxicity. Nevertheless, CS exhibits solubility exclusively in acidic solutions. Consequently, amino groups exhibit low protonation ability in alkaline environments **(Konios *et al.,* 2014)**, rendering the removal procedure ineffective. Additionally, CS exhibits poor mechanical qualities and can deteriorate with time **(Chang *et al.,* 2015)**. These limitations restricted its extensive utilization. Chitosan can undergo crosslinking or grafting processes **(Kyzas & Lazaridis, 2009)** to create a robust and effective substance that may be used across a wide range of pH levels.

Hydrogels are three-dimensional polymeric networks consisting of water-soluble polymer chains connected by physical or chemical connections. In the presence of water, hydrogels can swell to a significantly greater weight than their original dry weight, depending on the degree of crosslinking **(Adelnia *et al.,* 2019)**. Chitosan-based hydrogels have been utilized in several fields, including water treatment, and are particularly favored in wastewater treatment due to their high adsorption capacity, affordability, rapid kinetics, and ability to be reused. They can remove contaminants by attracting them through an electrostatic contact, a hydrogen bonding, or complexation, which depends greatly on their chemical structure **(Pakdel & Peighambardoust, 2018)**. Chitosan-based hydrogels have recently demonstrated a strong ability to remove emerging contaminants **(Basheer, 2018)**.

Driven by the remarkable characteristics of chitosan and magnetite nanoparticles, this study aimed to create a magnetic chitosan hydrogel that is cross-linked using glutaraldehyde. Different types of water were treated by the prepared hydrogel. Water quality criteria was examined before and after treatments.

MATERIALS AND METHODS

1. Experimental protocol

1.1. Synthesis of magnetite nanoparticles

Magnetite nanoparticles were synthesized by the wet chemical reduction technique (**Chaki *et al.,* 2015**). In brief, 50ml of $NaBH_4$ solution (2.5 M) was prepared in a beaker using magnetic stirring. Then, 40ml of 0.1 M ferric chloride solution was added dropwise to the first solution while vigorously stirring. The resultant solution darkened gradually when the ferric chloride solution was added until it became completely black. The addition of full ferric chloride resulted in black precipitates in less than 1 minute. The reaction was characterized by the formation of bubbles. When bubble creation ended, the reaction was assumed to be complete. The magnetite nanoparticles were filtered and washed numerous times with distilled water and 100% methanol. The particles were oven-dried overnight at 50°C.

1.2. Synthesis of magnetic CS-HG

Chitosan (1g) was dissolved in 100ml of glacial acetic acid (1%) and allowed to stir until a homogenous mixture was obtained. Then 1 gram of magnetic nanoparticles were added to the CS solution and allowed to stir till complete homogeneity. Solution of 1% glutaraldehyde was added to the homogeneous mixture within 30min of a continual stirring. To obtain the hydrogel, 100ml of pure ethyl alcohol was added while stirred continuously for 12hr to remove any excess glutaraldehyde. The resultant hydrogel was washed by ethyl alcohol several times in a sonication bath. After washing, it was preserved in the refrigerator till usage.

1.3. Characterization of magnetite nanoparticles and magnetic CS-HG

FT-IR: FT-IR spectrum was recorded on a BRUKER Tensor-37 FT-IR spectrophotometer in the range of 4000– 400cm^{-1} as a KBr disc. FT-IR was applied to characterize the presence of specific functional groups on the surface of prepared compounds.

Zeta potential: Zeta potential is one of the most important parameters for the stability of nanoparticles. Zeta potential analysis was prepared with a constant concentration of 1% (w/v). Three measurements were made for each sample, and the mean was reported as the zeta-potential value of the sample.

SEM and EDX: The shape and morphology of magnetite NPs were determined by SEM. Samples were labelled with a gold monolayer (sputter coating), and the scanning was done in the region of 2θ from 30 to 80 at 0.041/min with a time constant of 2s. EDX was used to ascertain the elemental composition.

XRD: The crystal structure of CS, magnetic NPs, and magnetic CS-HG were characterized by XRD. XRD was obtained using a powder Rigaku X-ray diffractometer (PXRD; Rigaku, Japan). The scanning was done in the region of 2θ from 30 to 80 at 0.041/ min with a time constant of 2s.

1.4. Water sampling

Different sources of water were collected from the aquaculture system established at the wet laboratory, NIOF, Suez and Aqaba Gulfs Branch, and summarized in Table (1).

Table 1. Different sources of water that used in the study

Sample no.	Source
1	Saline water: Filtered seawater
2	Saline water: Shrimp culture effluents (Shrimp fed with 42% crude protein for 3 months)
3	Freshwater: Nile Tilapia culture effluents (Tilapia fed with 40% crude protein for 4 months)
4	Normal tap water

1.5. Water quality measurements

Water quality criteria (temperature, total suspended solids, turbidity, pH, conductivity, dissolved oxygen, biological oxygendemand, nitrite, nitrate, ammonium/ammonium, phosphate, and heavy metals) were performed according to standard methods **(APHA, 2023)**, as follows:

Temperature (°C): Wastewater temperature, up to 0.01 accuracy, was measured *in situ* by an inductive portable thermometer.

Total suspended solids (TSS): The HACH DR 2010 spectrometer was used to measure TSS at the wavelength of 810nm. The measurement was conducted according to Method 8006, Programme No. : 630 **(DR, 2010a)**.

Turbidity: Turbidity measurements were taken at a wavelength of 860nm using the HACH DR 2010 spectrometer. This was done according to Method 8237, Programme No.: 750 **(DR, 2010b)**.

Hydrogen-ion concentration (pH): The pH of water samples was promptly measured in the laboratory using a benchtop ADWA 8000 Electrochemistry Analyzer pH meter. The instrument has a reading accuracy of up to 0.01 pH unit. Precautions were taken during the sampling and standardization operations.

Conductivity: The conductivity of water samples was measured immediately in the laboratory after collection using a bench-type conductivity meter (Orion 3 Star).

Dissolved oxygen (DO): DO determination was carried out by the classical Winkler's method modified by **Grasshoff (1976)**.

Biological oxygen diamond (BOD): The protocols to collect samples for BOD testing follow the identical processes outlined for measuring dissolved oxygen (Winkler's method), with one notable distinction. At each tank, a secondary sample was obtained using a BOD bottle and transported to the laboratory for dissolved oxygen (DO) analysis following a 5-day incubation period (at 20°C). The biochemical oxygen demand (BOD) was quantified in milligrammes per liter of dissolved oxygen (DO), as specified by the American Public Health Association **(APHA, 2023)**.

Nitrite (NO_2^-), nitrate (NO_3^-), ammonia/ammonium (NH_3/NH_4^+), and phosphate (PO_4^{3-}) were measured calorimetrically, following the method described in **APHA (2023)** by using UV-visible double beam spectrophotometer (Jenway 6800).

Heavy metals: The ammonium pyrrolidinedithiocarbamate - methyl isobutyl ketone extraction approach was used to determine the presence of heavy metals, using the standard protocols outlined in **APHA (2023)**. The contents of zinc and iron were determined using a flame atomic absorption spectrophotometer (FAAS; Perkin Elmer A Analyst 100). The concentrations of zinc and iron were reported in milligrams per liter (mg/ L).

1.6. Bacterial count of water samples after and before processing

Initial sample collection involved water samples of aquaculture waste using trypticase soy broth & agar (total bacterial count), Pseudomonas agar (*pseudomonas* sp.), TCBS agar (*Vibrio* sp.) and Aeromonas agar (*Aeromonas* sp.) medium **(Nair, 2016)**. To reduce the number of bacterial isolates in agar for the possibility of counting, a serial dilution technique was employed. A 10-fold dilution series of samples was created using sterile distilled water. From each dilution, 200µl was plated onto TS agar. After 24h of incubation, the plates were observed and counted. Moreover, the bacterial count per ml was calculated **(Ben-David & Davidson, 2014)**.

1.7. Identification of aquaculture-isolated pathogens

The genomic DNA extraction from freshly incubated Pseudomonas isolates was conducted using a suitable DNA extraction kit (Qiagen) following the manufacturer's instructions, ensuring the production of high-quality DNA with a 260/280 nm ratio within the range of 1.8 to 2.0. The amplification of genes was initiated through the setup of a polymerase chain reaction (PCR) using universal primers such as 27F (5'-AGAGTTTGATCMTGGCTCAG-3') and 1492R (5'-GGTTACCTTGTTACGACTT-3'). Subsequently, the analysis of PCR products involved their application on an agarose gel to confirm successful amplification. To purify the PCR products, a PCR purification kit (Qiagen PCR Purification Kit) was employed to effectively remove primers and

nucleotides. The resulting purified PCR products were then subjected to Sanger sequencing to acquire the complete 16S rRNA gene sequence. Sequence alignment was performed using bioinformatics tools against databases like NCBI for the identification of bacterial species and accession number registration. To visualize the evolutionary relationships of the identified Pseudomonas isolates, the construction of a phylogenetic tree was executed using software such as MEGA (Molecular Evolutionary Genetics Analysis). This methodological approach ensures a systematic and accurate identification process through multiple steps, from DNA extraction to phylogenetic analysis **(Ghiasian *et al.*, 2017)**.

RESULTS

1. Characterization of synthesized magnetic nanoparticles and magnetic CS-HG

Magnetite nanoparticles were synthesized by the wet chemical reduction technique and obtained as a black powder attracted to the magnet. However, magnetic CSMG-HG was synthesized and obtained as a thick brown hydrogel.

FT-IR: The synthesized magnetic nanoparticles and magnetic CS-HG were characterized by FT-IR analysis. It was observed in the FT-IR spectrum (Fig. 1) that CS showed: (a) a very strong broad peak at $3376cm^{-1}$ assigned to hydroxyl (-OH) groups, (b) a strong sharp peak at $1653cm^{-1}$ assigned to amide I of the acetylated amino group (-NHCOCH$_3$), (c) a strong sharp peak at $1599cm^{-1}$ assigned to N-H bending of NH$_2$ group, and (d) very strong sharp peak at $1159cm^{-1}$ assigned to C-O-C stretching vibration of the glycosidic linkage. Magnetite NPs showed two strong peaks between 560 and $450cm^{-1}$ attributed to the stretching vibration of Fe – O bonds in the crystal lattice of Fe$_3$O$_4$ **(Waldron, 1955; Bordbar, 2014)**. Moreover, two characteristic peaks due to adsorbed water molecules appeared **(Silva *et al.*, 2020)**, a strong broad peak at 3380 was related to –OH stretching vibration and a strong sharp peak at 1630cm-1 was related to –OH bending. Comparing magnetic CS-HG with CS and magnetite NPs, it was observed in Fig.(1) that magnetic CS-HG shows (a) a strong broad peak at $3430cm^{-1}$ assigned to –OH stretching vibration (intermolecular hydrogen bond), (b) a strong sharp peak at $2917cm^{-1}$ assigned to –CH stretching vibration, (c) medium broad bands at 1573 and $1425cm^{-1}$ assigned to amide I and II of the acetylated amino group (-NHCOCH$_3$), and (d) a peak at $1068cm^{-1}$ assigned to C-O stretching vibration, which were the main characteristic peaks of CS. Additionally, it showed two strong broad peaks overlapped between 630 and $605cm^{-1}$ assigned to the stretching vibration of Fe – O bonds which are characteristic of magnetite NPs. In addition, a medium sharp peak at 1625 m^{-1} was assigned to C=N stretching vibration.

Zeta potential: The zeta potentials of magnetite nanoparticles and magnetic CS-HG are shown in Fig. (2). The results indicated that the surface charge on magnetite nanoparticles and magnetic CS-HG was the same (-26± 0.1 mV).

SEM and EDX analysis: The morphology of the magnetic CS-HG sample was analyzed using the SEM technique and compared to that of CS. This comparison is shown in Fig. (3). The CS material displayed a coarse texture with an uneven surface **(Mustafa *et al.,* 2023)**. However, after being transformed into magnetic CS-HG, the surface became more distinct and uniform, characterized by many grains. Furthermore, the elemental compositions were determined via the EDX approach. The primary constituents of CS and magnetic CS-HG were carbon (C), nitrogen (N), and oxygen, as indicated in Table (2). The elemental composition of magnetic CS-HG showed an increasing percentage of iron (Fe) (31.85%) and decreasing ratios of C, N, and O.
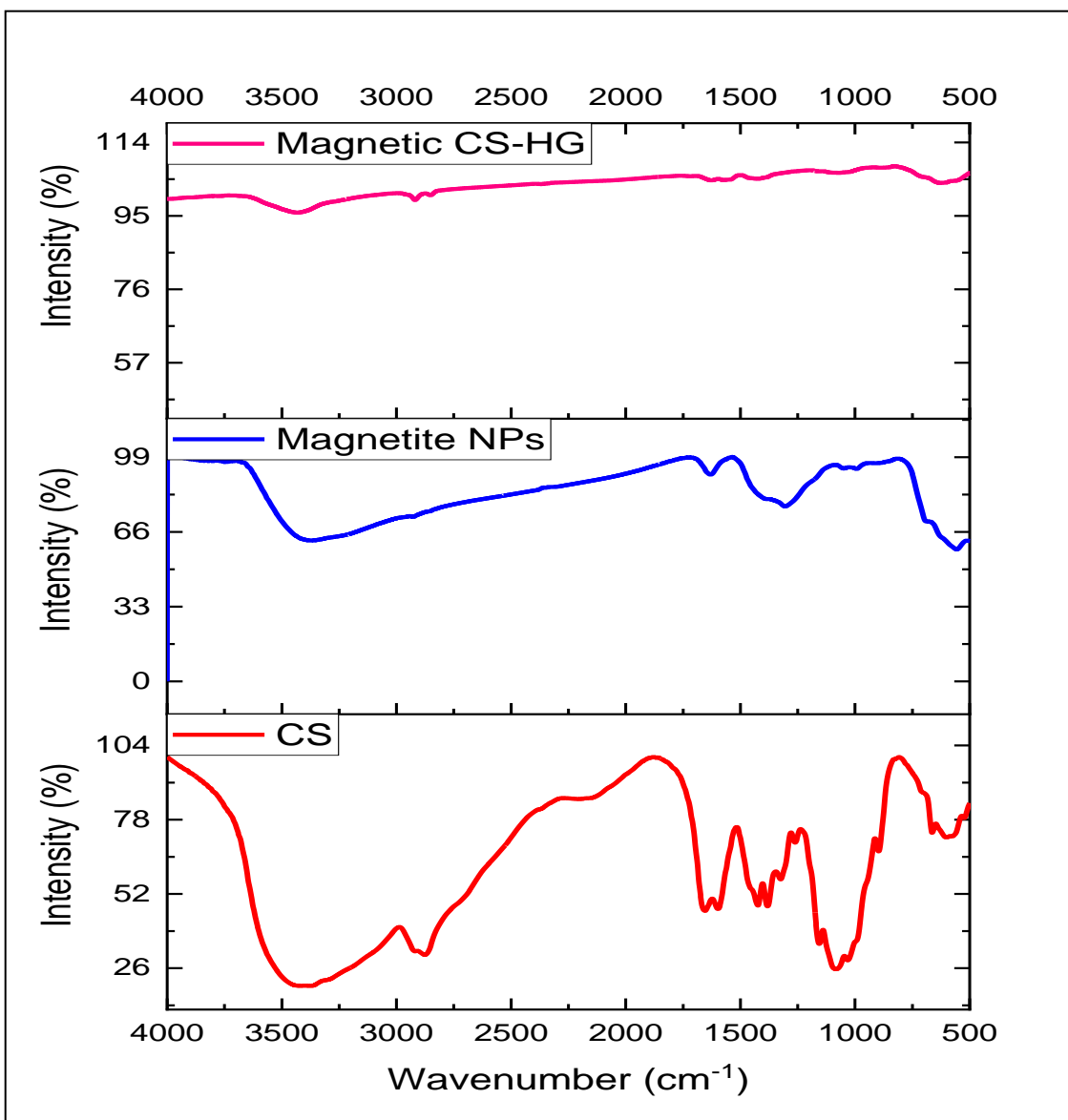
**Fig. 1.** FT-IR spectra of CS, magnetite, and magnetic CS-HG
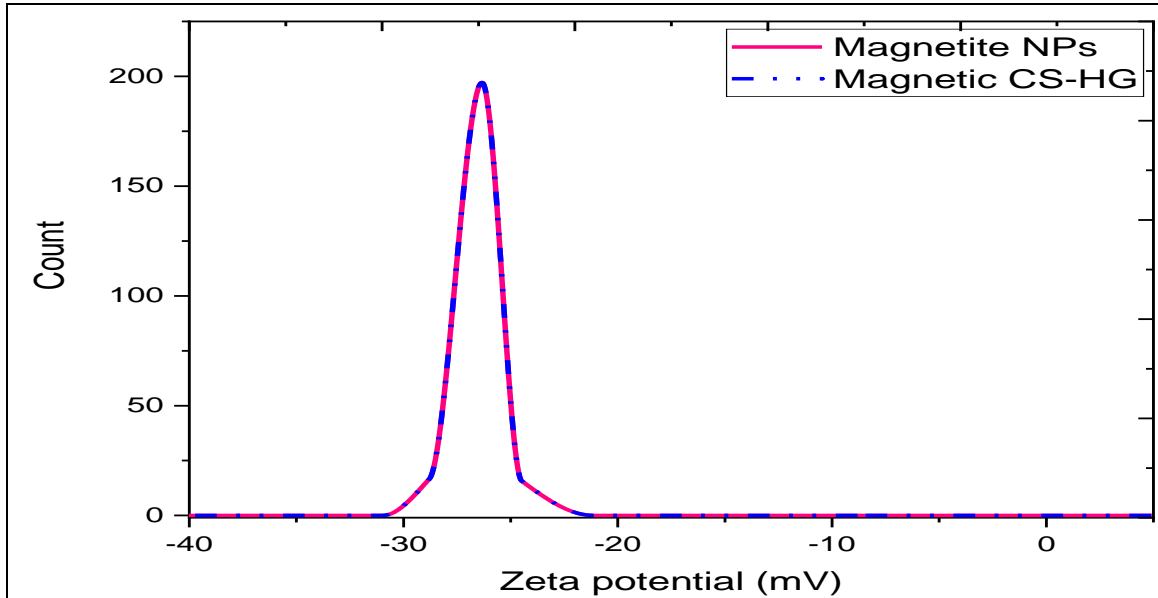
Fig. 2. Zeta potential analysis of magnetite NPs and magnetic CS-HG
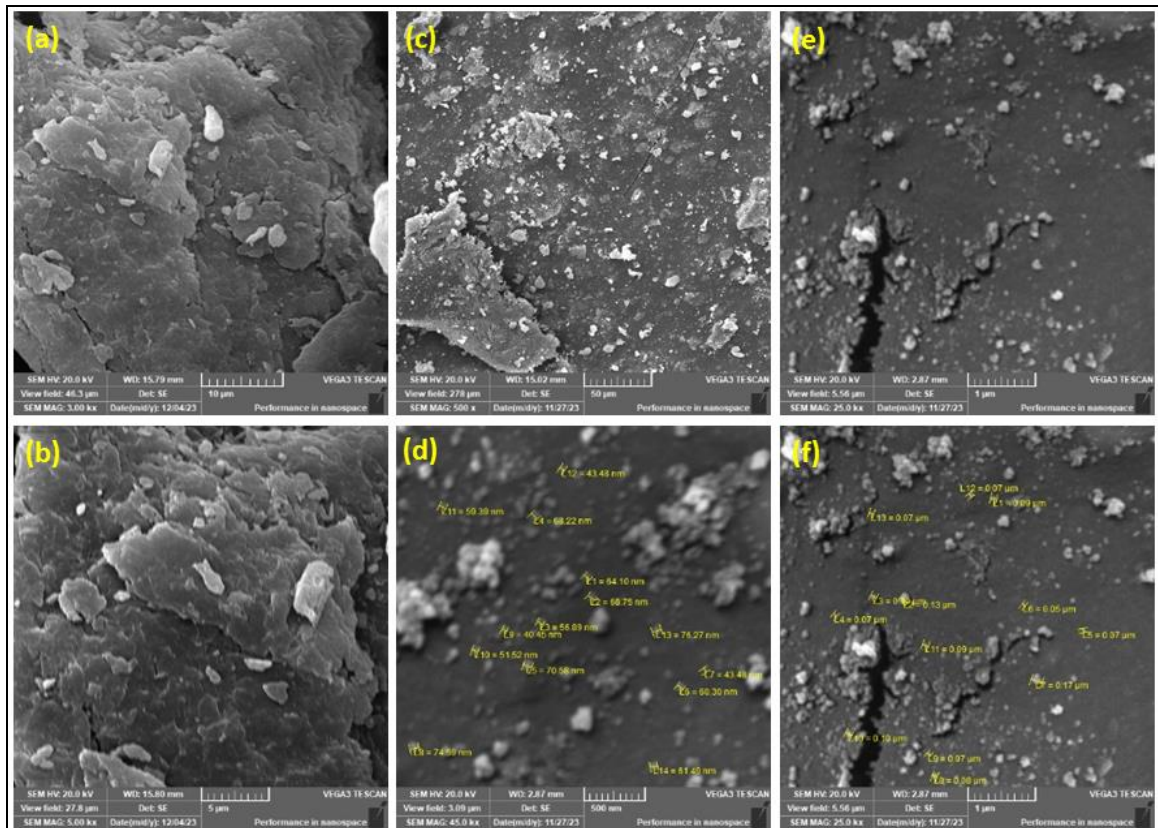
Fig. 3. SEM analysis showing surface topographies of CS (a and b) and magnetic CS-HG (c, d, e, and f)

XRD: XRD patterns of CS, magnetite NPs and magnetic CS-HG are shown in Fig. (4). CS showed low-intensity broad peaks at $2\theta \approx 19°$ and $40°$. However, magnetite NPs showed strong sharp diffraction peaks recorded at $2\theta = 25.23°$, $26.93°$, $31.07°$, $40.91°$, $42.75°$, $49.79°$, $59.01°$, $70.97°$. In addition, magnetic CS-HG showed sharp diffraction peaks recorded at $2\theta = 24.77°$, $26.73°$, and $41.51°$.
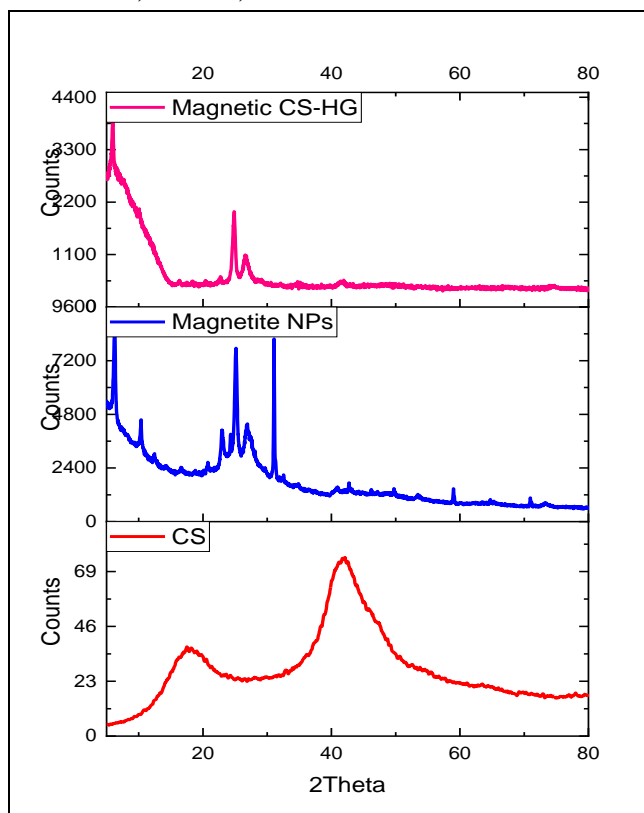
Fig. 2. XRD of CS, magnetite NPs and magnetic CS-HG

Table 2. Chemical composition of EDX analysis

Material	Weight %			
	C	**N**	**O**	**Fe**
CS	42.01	18.20	39.78	-
Magnetic CS-HG	36.57	1.58	30	31.85

2. Water quality

Wastewater samples were collected from fish pond (sample 3) and shrimp pond (sample 2) in aquaculture experiments which compared to the saline water source (sample 1) and tape water source (sample 4) used at the beginning of the aquaculture experiments. These samples were analyzed before and after treatment with magnetic chitosan hydrogel. The samples were treated under the ideal conditions established in earlier research, which included a pH of 1.2, a temperature of $35^{o}C$, a treatment period of

20 minutes, a dosage of 0.5g, and a rotation speed of 150 revolutions per minute. These conditions were chosen to assess the potential use of the samples. Table (3) presents a concise overview of the water quality findings obtained before and following the application of remedies.

Regarding sample 1, magnetic CS-HG had significantly removed iron, total inorganic phosphate, total phosphate, and TSS, with efficiencies reaching 98.39, 90.91, 85.71, and 85.86%, respectively. Moreover, it had moderate removal efficiencies of turbidity, orthophosphate, nitrate, and nitrite (73.08, 66.67, 67.86, and 45.48%, respectively). It also removed ammonia/ammonium with an efficiency reaching 34.35%. For sample 2, magnetic CS-HG showed high removal efficiencies towards nitrite, nitrate, and iron (95.17, 93.40, and 97.87%, respectively). Additionally, it had moderate efficiencies against turbidity, TSS, and orthophosphate (66.67, 68.69, and 50.00%, respectively). In addition, it removed ammonia/ammonium, phosphate, and zinc with efficiencies reaching 36.76, 23.08, and 28.57%, respectively. In sample 3: Magnetic CS-HG showed high removal efficiencies towards turbidity, TSS, phosphate, inorganic phosphate, and orthophosphate (88.16, 98.27, 85.19, 86.67, and 77.78%, respectively). In addition, it had moderate efficiencies against turbidity of 49.65%. Furthermore, it removed nitrate and iron with efficiencies reached 10.06 and 42.03%, respectively. For sample 4, magnetic CS-HG showed high efficiencies in removing TSS, nitrite, nitrate, and iron (78.33, 92.25, 84.74, and 99.17%, respectively). It also showed moderate efficiencies (57.14 and 49.58%) towards removing turbidity and ammonia/ammonium. Moreover, it had reasonable removal efficiencies toward phosphate, inorganic phosphate, and orthophosphate phosphate reaching 30.00, 33.33, and 25.00%, respectively.

By comparing the gel's efficiency against each pollutant in the four samples, the highest efficiencies for removing turbidity, TSS, total phosphate and orthophosphate (88.16, 98.27, 85.71 and 77.78%, respectively) were recorded in sample 3. In addition, the highest efficiencies for removing nitrite, nitrate and zinc (95.17, 93.4, and 28.57%, respectively) were recorded in sample 2. In addition, the highest efficiencies for removing ammonia/ammonium and iron (49.58 and 99.17%, respectively) were recorded in sample 4. Moreover, the highest efficiency for removing total inorganic phosphate 90.91 % was recorded in sample 1. However, the lowest efficiencies for removing TSS, total phosphate and inorganic phosphate (68.69, 23.08, and 11.11%, respectively) were recorded in sample 2. Moreover, the lowest efficiencies for removing nitrite, ammonia/ammonium and zinc (45.48, 34.35, and 13.33%, respectively) were recorded in sample 1. In addition, the lowest efficiencies for removing turbidity and orthophosphate (57.14 and 25%, respectively) were recorded in sample 4. Furthermore, the highest efficiency for removing nitrate and iron (10.06 and 42.03%, respectively) was recorded in sample 3.

Table 3. Effect of magnetic CS-HG treatments on water quality

Parameter	Sample 1		Reduction (%)	Sample 2		Reduction (%)	Sample 3		Reduction (%)	Sample 4		Reduction (%)
	Before	After		Before	After		Before	After		Before	After	
pH	8.26	7.00	15.25	7.70	7.00	9.09	9.28	7.00	24.57	7.55	7.00	7.29
Conductivity (µs)	57.00	58.11	-1.95	61.00	61.05	-0.08	1213.00	1320.00	-8.82	574.00	576.00	-0.35
Turbidity (NTU)	26.00	7.00	73.08	21.00	7.00	66.67	76.00	9.00	88.16	7.00	3.00	57.14
TSS (ppm)	6.01	0.85	85.86	3.13	0.98	68.69	45.00	0.78	98.27	4.06	0.88	78.33
Nitrite (ppm)	2.15	1.17	45.48	43.52	2.10	95.17	2.10	1.06	49.65	2.10	0.16	92.25
Nitrate (ppm)	2.31	0.74	67.84	40.22	2.65	93.40	1.50	1.35	10.06	0.60	0.09	84.74
Ammonia/Ammonium (ppm)	0.61	0.40	34.35	0.64	0.40	36.76	0.75	0.40	46.51	0.11	0.06	49.58
Total PO4 3- (ppm)	1.40	0.20	85.71	1.30	1.00	23.08	5.40	0.80	85.19	1.00	0.70	30.00
Total Inorganic PO4 3- (ppm)	1.10	0.10	90.91	0.90	0.80	11.11	4.50	0.60	86.67	0.60	0.40	33.33
Orthophosphate PO4 3- (ppm)	0.30	0.10	66.67	0.40	0.20	50.00	0.90	0.20	77.78	0.40	0.30	25.00
Iron (ppm)	0.62	0.01	98.39	0.47	0.01	97.87	0.69	0.40	42.03	1.20	0.01	99.17
Zinc (ppm)	0.15	0.13	13.33	0.07	0.05	28.57	0.06	0.06	0.00	0.06	0.06	0.00

3. Bacterial count of aquaculture water samples after and before processing

The result of bacterial count includes total bacterial count, *Pseudomonas* sp., *Vibrio* sp. and *Aeromonas* sp. The bacterial counts before and after the chemical treatment process were evaluated for each of the specified bacterial types and presented in Table (4), including total coliforms (TC), *Pseudomonas* (Pseud), *Aeromonas* (Aer), and *Vibrio* (Vib). The following observations were made based on the provided data:

The initial bacterial count of TC in the samples ranged from 600,000 to 5,500,000 CFU/ mL. After undergoing the chemical treatment process, the TC counts were reduced significantly to a range of 4,000 to 60,000 CFU/ ml. This indicates a substantial decrease in TC bacterial populations following the chemical treatment. *Pseudomonas* bacterial counts before processing ranged from 0 to 25,000 CFU/ ml. Post-processing, the Pseud counts were notably reduced, with values ranging from 50 to 75 CFU/ ml. This indicates that the chemical treatment effectively decreased Pseud populations in the samples. The initial counts of Aer and Vib bacteria were recorded as 0 CFU/ ml before processing. These counts remained unchanged after the chemical treatment, so far these specific bacterial types have not been detected in the samples either before or after the treatment.

Table 4. The count of bacterial species after and before processing (CFU/ml)

| Sample no.	Before processing				After processing			
	TC	Pseud	Aer	Vib	TC	Pseud	Aer	Vib
1	5500000	22000	0	0	60000	75	0	0
2	600000	250	0	0	4000	5	0	0
3	1400000	25000	0	0	9500	70	0	0
4	3800000	8000	0	0	28500	50	0	0

4. Identification of bacterial isolates

The results of the identification of the bacterial isolates with their respective accession numbers are represented in Table (5). The bacterial isolates *Pseudomonas* sp. 1, 2, 4 and 6 were identified as *Neobacillus novalis* -AQUA1, *Psychrobacillus lasiicapitis* -AQUA2, *Acinetobacter schindleri* -AQUA4 and *Bacillus paramycoides* AQUA6 with the accession number OR805131, OR810726, OR810933 and OR794156, respectively.

**Table 5.** Genetic identification of pathogenic strains with accession number

Isolate	Identification accession number
Pseudomonas **sp. 1**	*Neobacillus novalis* AQUA1 -OR805131
Pseudomonas **sp. 2**	*Psychrobacillus lasiicapitis* AQUA2 - OR810726
Pseudomonas **sp. 4**	*Acinetobacter schindleri* AQUA 4 - OR810933
Pseudomonas **sp. 6**	*Bacillus paramycoides* AQUA 6 - OR794156

The results of the tree show that the *Neobacillus novalis* strains are most closely related to each other, and form a distinct clade. This clade is sister to a clade containing *Bacillus novalis* and *Mesobacillus foraminis*. The *Caldibacillus debilis* strains are more distantly related to the other bacteria in the tree. The branch lengths in the tree can be interpreted as estimates of evolutionary distance, with longer branches indicating more time since two lineages diverged from a common ancestor. For example, the branch leading to the *Neobacillus novalis* clade is longer than the branch leading to the *Bacillus novalis* and *Mesobacillus foraminis* clade, suggesting that the *Neobacillus novalis* strains diverged from their common ancestor with the other bacteria earlier in evolutionary history (Fig. 5).
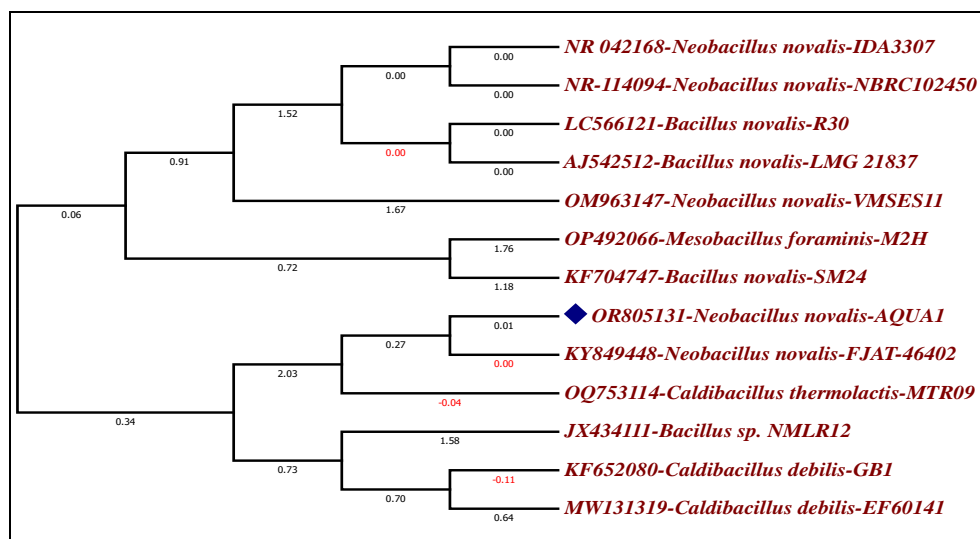
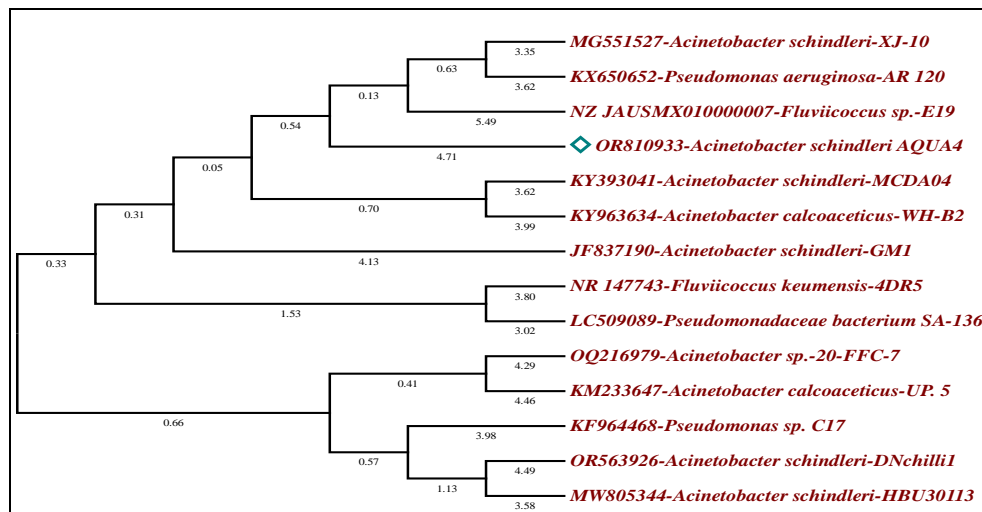**Fig. 5.** The phylogenetic tree of *Neobacillus novalis* -AQUA1

Regarding the phylogeny of *Psychrobacillus lasiicapitis* -AQUA2, the strains were clustered into three main groups. The first group consists of two *Psychrobacillus lasiicapitis* strains (OR144256 and LC769518). These strains are very closely related, with a bootstrap support value of 90%. This suggests that they diverged from a common ancestor relatively recently. The second group contains five strains, three *Psychrobacillus*

lasiicapitis strains (OP854820, OR763717, and OM971298), one *Psychrobacillus psychrodurans* strain (KT937150), and one *Psychrobacillus* sp. strain (KT715741). These strains are also relatively closely related, with bootstrap support values ranging from 79 to 89%. The third group is more diverse and includes four strains, two *Psychrobacillus lasiicapitis* strains (OR810726 and OQ581748), one *Bacillus salipaludis* strain (MK627545), and one *Bacillus* sp. strain (MH718307). These strains are more distantly related to each other than the strains in the other two groups, with bootstrap support values ranging from 62 to 97% (Fig. 6).
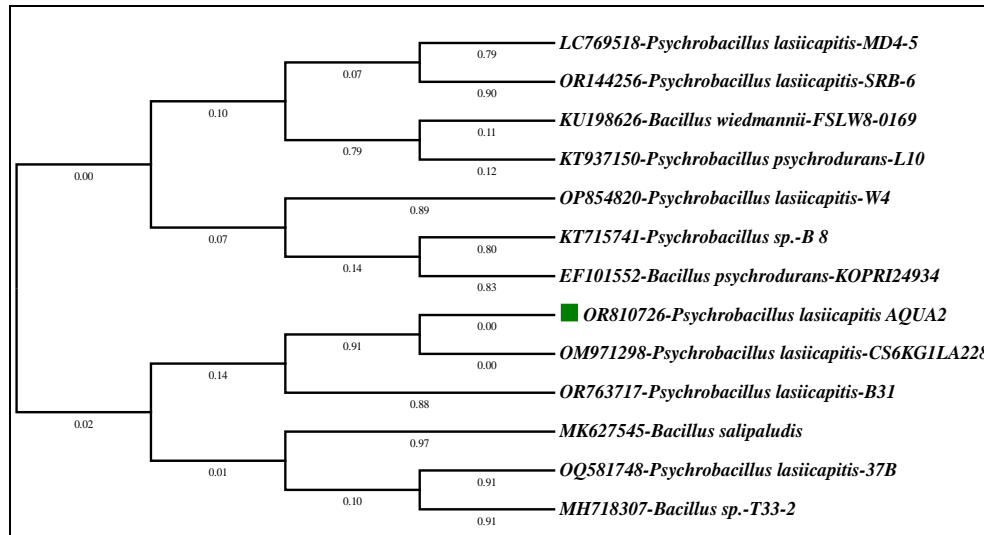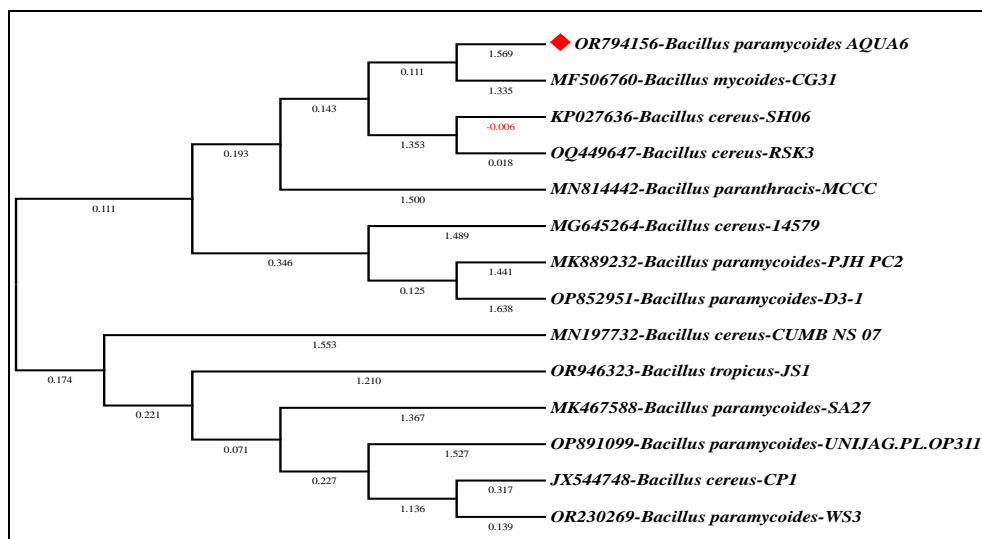

Fig. 6. The phylogenetic tree of *Psychrobacillus lasiicapitis* -AQUA2

The phylogenetic tree of *Acinetobacter schindleri* -AQUA4 is divided into two main groups. The first branch contains all of the *Acinetobacter schindleri* strains, as well as one strain of *Pseudomonas aeruginosa* -KX650652. This suggests that these strains are more closely related to each other than they are to the other strains in the tree. The second branch contains strains of *Pseudomonas aeruginosa*, *Fluviicoccus keumensis*, and *Acinetobacter calcoaceticus*. This suggests that these strains are more closely related to each other than they are to the *Acinetobacter schindleri* strains (Fig. 7).

Fig. 7. The phylogenetic tree of *Acinetobacter schindleri* -AQUA4.

The phylogeny of *Bacillus paramycoides* -AQUA6 is grouped into four categories, first group consists of two closely related *Bacillus paramycoides* strains. Second group contains four *Bacillus cereus* strains and one *Bacillus mycoides* strain. The third group is more diverse and includes five strains, two *Bacillus cereus* strains, one *Bacillus paramycoides* strain, one *Bacillus anthracis* strain, and one *Bacillus thuringiensis* strain. The fourth group is the most diverse and includes four strains, one *Bacillus cereus* strain two *Bacillus paramycoides* strains and one *Bacillus tropicus* strain (Fig. 8).

Fig. 8. The phylogenetic tree of *Bacillus paramycoides* -AQUA6

DISCUSSION

Chitosan has -OH and -NH$_2$ groups in its skeleton that allow chemical modification via many reactions **(Sheng *et al.,* 2004)**. Chemical modification aims to improve hydrogel characteristics and functions. Glutaraldehyde is a common cross-linker used to prepare the magnetic CS-HG. Glutaraldehyde initiates a cross-linking process targeting –NH$_2$ groups within the CS skeleton by forming covalent bonds. The overall reaction is a Schiff base condensation and glutaraldehyde acts as a bridge connecting chitosan polymeric chains generating a 3D network **(Lagergern, 1898)**. In the present study, different structural characteristics of synthesized magnetic nanoparticles and magnetic CS-HG were studied.

For FT-IR, the main characteristic peaks of CS, e.g. amide I, II (-NHCOCH$_3$) stretching appeared in the magnetic CS-HG spectrum **(Youssef Moustafa *et al.,* 2024)**. This confirms the participation of CS in the magnetic CS-HG network. However, a new peak assigned to the C=N group appeared in the spectrum of magnetic CS-HG confirming the condensation reaction between the primary amine group in CS and the aldehyde group in glutaraldehyde **(Mustafa *et al.,* 2023)**. Moreover, the stretching vibration peak attributed to Fe – O bonds in magnetite NPs spectrum was shifted to a high-frequency shift in the spectrum of magnetic CS-HG. This confirms the participation of magnetite NPs in the magnetic CS-HG network. All of the above demonstrates and proves the successful preparation of magnetite and magnetic CS-HG.

One of the physical properties that affects stability is the particle zeta potential. Zeta potential was used to quantify electric charge (electrostatic, repulsion, attraction) on the surface of magnetite nanoparticles. The average surface charge on magnetite nanoparticles and magnetic CS-HG was -26± 0.1mV, i.e., the zeta potential was in the negative direction. This gives evidence that the dispersion stability of the particles increased **(Lee *et al.,* 2020)**.

While for both scanning electron microscopy (SEM) and energy dispersive X-ray (EDX) analysis, there are differences in the surface morphologies of CS and magnetic CS-HG. Many grains appeared in SEM images of magnetic CS-HG. These grains indicate the incorporation of magnetic nanoparticles in the magnetic CS-HG matrix. In addition, the elemental compositions of magnetic CS-HG hydrogel were confirmed using the EDX technique, as iron amounts were observed as a major element in the magnetic CS-HG composition.

The XRD broad peaks of CS prove its amorphous nature. However, magnetite sharp diffraction peaks corresponded to the crystalline planes of the magnetite phase **(Compeán-Jasso *et al.,* 2008; Ouyang *et al.,* 2015)**. In addition, the sharp diffraction peaks of magnetic CS-HG confirm the incorporation of magnetite NPs in the matrix of magnetic CS-HG.

It is imperative to assess the effectiveness of the magnetic hydrogel in a real-world multi-pollutant environment that accurately replicates actual watery effluents, as opposed to simulated ones. The results revealed variant efficiencies toward different pollutants.

Magnetic hydrogel showed an efficient trend against different pollutants, especially iron, phosphates, nitrate, and nitrite. These results follow **Sharifi et al. (2021)**, who stated that chitosan-based nanocomposites have a higher potential for the adsorption of dyes, and metal ions, thus they might be a good alternative to remove pollutants from water and wastewater.

The reasons for such activities of magnetic CS-HG are the cationic character of CS polymer **(Sharifi et al., 2023)** and the negative charges on the magnetite nanoparticle surface. However, moderate efficiencies in ammonia/ammonium removal were noticed. This may be due to the competition between ammonia/ammonium and other pollutant molecules on the active sites that exist on the surface of the magnetic hydrogel. Thus, magnetic CS-HG could be applied to clean up different kinds of water.

The bacterial count after chemical processing demonstrates a considerable reduction in bacterial counts, particularly for total coliforms and *Pseudomonas*, following the chemical treatment process **(Lejri et al., 2022)**. The treatment proved effective in decreasing bacterial populations in the samples, enhancing the water quality in terms of microbial load. Additionally, the absence of detectable *Aeromonas* and *Vibrio* bacterial populations highlights the potential efficacy of the treatment in managing these specific bacterial types as well. These findings underscore the significance of chemical treatment as a method for mitigating bacterial populations and improving the overall quality of the samples in an aquaculture setting.

The identifications of isolates provide specific information about the microbial species associated with each *Pseudomonas* sp. isolate **(Caldera et al., 2016)**. The accession numbers serve as unique identifiers for the particular strains identified during the study. The tree analysis includes bootstrap support values, which are a measure of how confident we can be in the branching order of the tree. Bootstrap values of 70% or higher are generally considered to be good support for a particular branching pattern. In this tree, all of the major branches have bootstrap support values of 90% or higher, indicating that the tree is well-supported by the data. The results of the phylogenetic tree suggest that the *Neobacillus novalis* strains are a distinct group of bacteria that are closely related to, but distinct from, *Bacillus novalis* and *Mesobacillus foraminis*. The *Caldibacillus debilis* strains are more distantly related to the other bacteria in the tree. The tree provides a useful starting point for understanding the evolutionary relationships between bacterial strains **(Soltis & Soltis, 2003)**.

CONCLUSION

The magnetic chitosan hydrogel (CS-HG) nanocomposite was prepared and thoroughly characterized. Magnetic hydrogel showed high efficiencies in removing nutrient load and iron from different water types. Magnetic CS-HG could be applied to aquaculture farms to reduce pollution load on the marine environment. It also effectively

reduced bacterial load in the water samples, particularly for targeted groups like total coliforms and *Pseudomonas* sp. However, identification of bacterial isolates revealed that some initially classified as *Pseudomonas* sp. belong to different genera. Future research on synthetic compounds with promising antimicrobial and antibiofilm properties offers a potential avenue for combating these newly identified bacteria in aquaculture settings.

ACKNOWLEDGEMENT

REFERENCES

Abbas, E.M.; Al-Souti, A.S.; Sharawy, Z.Z.; El-Haroun, E. and Ashour, M. (2023). Impact of dietary administration of seaweed polysaccharide on growth, microbial abundance, and growth and immune-related genes expression of The Pacific whiteleg shrimp (Litopenaeus vannamei). Life. 13(2), 344.

Adelnia, H.; Blakey, I.; Little, P.J. and Ta, H.T. (2019). Hydrogels Based on Poly (aspartic acid): Synthesis and Applications. Front. Chem., 7: 755.

Ahmad, A.; Abdullah, S.R.S.; Hasan, H.A.; Othman, A.R. and Ismail, N.I. (2021). Aquaculture industry: Supply and demand, best practices, effluent and its current issues and treatment technology. J. Environ. Manage., 287**:** 112271.

Ahmad, A.; Kurniawan, S.B.; Abdullah, S.R.S.; Othman, A.R. and Hasan, H.A. (2022). Contaminants of emerging concern (CECs) in aquaculture effluent: Insight into breeding and rearing activities, alarming impacts, regulations, performance of wastewater treatment unit and future approaches. Chemosphere, 290**:** 133319.

APHA, (2023). American Public Health Association, American Works Association, Water Environmental Federation. In: Lipps WC, Braun-Howland Baxter TE, eds. Standard methods for the examination of water and wastewater, 24th ed. Washington, DC.

Basheer, A.A. (2018). New generation nano-adsorbents for the removal of emerging contaminants in water. J. Mol. Liq. 261583-593.

Ben-David, A. and Davidson, C.E. (2014). Estimation method for serial dilution experiments. J. Microbiol. Methods, 107**:** 214-221.

Bordbar, A.K.; Rastegari, A.A.; Amiri, R.; Ranjbakhsh, E.; Abbasi, M. and Khosropour, A.R. (2014). Characterization of Modified Magnetite Nanoparticles for Albumin Immobilization. Biotechnol. Res. Int., 2014: 705068.

Caldera, L.; Franzetti, L.V.; Van Coillie, ; De Vos, P.; Stragier, P.; De Block, J. and Heyndrickx, M. (2016). Identification, enzymatic spoilage characterization and proteolytic activity quantification of *Pseudomonas spp.* isolated from different foods. Food Microbiology, 54: 142-153.

Chaki, S.H.; Malek, T.J.; Chaudhary, M.D.; Tailor, J.P.; Deshpande, M.P. (2015). Magnetite Fe_3O_4 nanoparticles synthesis by wet chemical reduction and their characterization, Adv. Nat. Sci: Nanosci. Nanotechnol., 6: 035009.

Chang, S. H.; Lin, H.T.V. ; Wu, G.J. and Tsai, G.J. (2015). pH Effects on solubility, zeta potential, and correlation between antibacterial activity and molecular weight of chitosan. Carbohydr. Polym., 134: 74-81.

Compeán-Jasso, M.E.; Ruiz, F.; Martínez, J.R. and Herrera-Gómez, A. (2008). Magnetic properties of magnetite nanoparticles synthesized by forced hydrolysis. Mate. Lett., 62(27): 4248-4250.

DR (2010a) spectrophotometer procedures manual, suspended solids, Photometric Method, page 811.

DR (2010b) spectrophotometer procedures manual, Turbidity, Attenuated Radiation Method (direct reading) page 853.

El-Sawy, M.A.; Ashry, O.A.; Abbas, E.M.; Sharawy, Z.Z. and Kelany, M.S. (2022). Potential Application of Agriculture by-Products in Heavy Metals Bioremediation. Egypt. J. Aquat. Biol. Fish., 26(5), 53–67.

Ghiasian, M.; Akhavan, S.A.; Amoozegar, M.; Saadatmand, S. and Shavandi, M. (2017). Bacterial diversity determination using culture-dependent and culture-independent methods. GJESM, 3(2):153-164.

Gichana, Z.M.; Liti, D.; Waidbacher, H.; Zollitsch, W.; Drexler, S. and Waikibia, J. (2018). Waste management in recirculating aquaculture system through bacteria dissimilation and plant assimilation. Aquac. Int., 26: 1541-1572.

Grasshoff, K. (1976). Methods of Seawater Analysis, Verlage Chemie. Weinheim, NewYork, 317p.

Hamilton, P.B.; Cowx, I.G.; Oleksiak, M.F.; Griffiths, A.M.; Grahn, M.; Stevens, J.R.; Carvalho, G.R.; Nicol, E. and Tyler, C.R. (2016). Population-level consequences for wild fish exposed to sublethal concentrations of chemicals–a critical review. Fish Fish., 17: 545-566.

Hassan, S.A.H.; Sharawy, Z.Z.; El Nahas, A.F.; Hemeda, S.; El-Haroun, E. and Abbas, E.M. (2022a). Carbon sources improve water quality, microbial community, immune-related and antioxidant genes expression and survival of challenged *Litopenaeus vannamei* Postlarvae in biofloc system. Aquaculture Research, 53(17), 5902–5914.

Hassan, S.A.H.; Sharawy, Z.Z., El Nahas, A.F.; Hemeda, S.; El-Haroun, E. and Abbas, E.M. (2022b). Modulatory effects of various carbon sources on growth indices, digestive enzymes activity and expression of growth-related genes in

whiteleg shrimp, Litopenaeus vannamei reared under an outdoor zero-exchange system Aquaculture Research, 53(16), 5594–5605.

Jose Priya, T. and Kappalli, S. (2023). Chemicals and Their Interaction in the Aquaculture System. In Biomedical Applications and Toxicity of Nanomaterials, 277-297. Springer.

Konios, D.; Stylianakis, M.M. ; Stratakis, E. and Kymakis, E. (2014). Dispersion behaviour of graphene oxide and reduced graphene oxide. J. Colloid Interface Sci., 430: 108-112.

Kyzas, G.Z. and Lazaridis, N.K. (2009). Reactive and basic dyes removal by sorption onto chitosan derivatives, J. Colloid Interface Sci., 331: 32-39.

Lagergern, S. (1898). About the Theory of So-Called Adsorption of Soluble Substances. Kungl. Vetensk Acad. Handl., 24:1–39.

Lee, J.M.; Lim, D.S.; Jeon, S.H. and Hur, D.H. (2020). Zeta Potentials of Magnetite Particles and Alloy 690 Surfaces in Alkaline Solutions. Materials (Basel), 13(18): 3999.

Lejri, R.; Younes, S.B.; Ellafi, A.; Bouallegue, A.; Moussaoui, Y.; Chaieb, M. and Mekki, A. (2022). Physico-chemical, microbial and toxicity assessment of industrial effluents from the southern Tunisian tannery. JWPE., 47**:** 102686.

Mansour, A.T.; Ashry, O.A.; El-Neweshy, M.S.; Alsaqufi, A.S.; Dighiesh, H.S.; Ashour, M.; Kelany, M.S.; El-Sawy, M.A.; Mabrouk, M.M.; Abbas, E.M. and Sharawy, Z.Z. (2022a). Effect of Agricultural By-Products as a Carbon Source in a Biofloc-Based System on Growth Performance, Digestive Enzyme Activities, Hepatopancreas Histology, and Gut Bacterial Load of Litopenaeus vannamei Post Larvae. J. Mar. Sci. Eng., 10(10), 1333.

Mansour, A.T.; Ashour, M.; Abbas, E.M.; Alsaqufi, A.S.; Kelany, M.S.; El-Sawy, M.A. and Sharawy, Z.Z. (2022b). Growth Performance, Immune-Related and Antioxidant Genes Expression, and Gut Bacterial Abundance of Pacific White Leg Shrimp, Litopenaeus vannamei, Dietary Supplemented with Natural Astaxanthin. Front. Physiol., 13, 874172.

Mustafa, F.H.A.; Gad ElRab, E.Kh.M.; Kamel, R.M. and Elshaarawy, R.F.M. (2023). Cost-effective removal of toxic methylene blue dye from textile effluents by new integrated crosslinked chitosan/aspartic acid hydrogels. Int. J. Biol. Macromol., 248: 125986.

Nair, V.A. (2016). Bioprospecting of novel antimicrobial metabolites from *Bacillus subtilis* MBTDCMFRI Ba37 and *Pseudomonas aeruginosa* MBTDCMFRI Ps04 of tropical estuarine habitats of Cochin, India and its application in fish health management. ICAR-Central Marine Fisheries Research Institute. PhD Thesis.

Ouyang, Z.-W.; Chen, E.-C.; Wu, T.-M. (2015). Thermal Stability and Magnetic Properties of Polyvinylidene Fluoride/Magnetite Nanocomposites. Materials, 8: 4553-4564.

Pakdel, P.M.; Peighambardoust, S.J. (2018). Review on recent progress in chitosan-based hydrogels for wastewater treatment application, Carbohydr. Polym., 201: 264-279.

Sharawy,Z.Z.; Abbas, E.M.; Abdelkhalek, N.K.; Ashry, O.A.; Abd El-Fattah, L.S.; El-Sawy, M.A.; Helal, M. and El-Haround, E. (2022). Effect of organic carbon source and stocking densities on growth indices, water microflora, and immune-related genes expression of Litopenaeus vannamei Larvae in intensive culture. Aquaculture, 546, 737397.

Sharawy, Z.Z.; Thiele, R.; Abbas, E.M.; El-Magd, M.A.; Hassaan, M.S.; Peter, C.; Schmidt, J.; Saborowski, R.; Goda, A.M.A-S. and Slater, M.J. (2017). Antioxidant response, body composition of whiteleg shrimp Litopenaeus vannamei co-cultured with Nile tilapia Oreochromis niloticus in recirculating aquaculture. Aquaculture Environment Interaction. 9: 257-268.

Sharifi, M.J.; Nouralishahi, A.; Hallajisani, A. and Askari, M. (2021). Magnetic chitosan nanocomposites as adsorbents in industrial wastewater treatment: A brief review. group, 60: 61.

Sharifi, M.J.; Nouralishahi, A. and Hallajisani, A. (2023). Fe_3O_4-chitosan nanocomposite as a magnetic biosorbent for removal of nickel and cobalt heavy metals from polluted water. Int. J. Biol. Macromol., 248: 125984.

Sheng, P.X.; Ting, Y.-P.; Chen, J.P. and Hong, L. (2004). Sorption of lead, copper, cadmium, zinc, and nickel by marine algal biomass: characterization of biosorptive capacity and investigation of mechanisms. J. Colloid Interface Sci. 275(1): 131-141.

Silva, C.A.S. ; e Silva, R.L.S.; de Figueiredo, A.T. and Alves, V.N. (2020). Magnetic Solid-Phase Microextraction for Lead Detection in Aqueous Samples Using Magnetite Nanoparticles, J. Braz. Chem. Soc., 31(1): 109-115.

Soltis, P. S. and Soltis, D. E. (2003). Applying the bootstrap in phylogeny reconstruction. Statistical Science, 256-267.

Sundin, G.W., Castiblanco, L.F.; Yuan, X.; Zeng, Q. and Yang, C.H. (2016). Bacterial disease management: challenges, experience, innovation and future prospects: challenges in bacterial molecular plant pathology. Mol. Plant Pathol., 17: 1506-1518.

Waldron, R.D. (1955). Infrared Spectra of Ferrites. Phys. Rev., 99: 1727-1735.

Youssef Moustafa, A.M.; Fawzy, M.M.; Kelany, M.S.; Hassan, Y.A.; Elsharaawy, R.F.M. and Mustafa, F.H.A. (2024). Synthesis of new quaternized chitosan Schiff bases and their N-alkyl derivatives as antimicrobial and anti-biofilm retardants in membrane technology. Int. J. Biol. Macromol., 267(2): 131635.